

Anharmonic Lattice Dynamics from Vibrational Dynamical Mean-Field Theory

Petra Shih¹ and Timothy C. Berkelbach^{1,2,*}

¹*Department of Chemistry, Columbia University, New York, New York 10027, USA*

²*Center for Computational Quantum Physics, Flatiron Institute, New York, New York 10010, USA*

We present a vibrational dynamical mean-field theory (VDMFT) of the dynamics of atoms in solids with anharmonic interactions. Like other flavors of DMFT, VDMFT maps the dynamics of a periodic anharmonic lattice of atoms onto those of a self-consistently defined impurity problem with local anharmonicity and coupling to a bath of harmonic oscillators. VDMFT is exact in the harmonic and molecular limits, nonperturbative, systematically improvable through its clusters extensions, and usable with classical or quantum impurity solvers, depending on the importance of nuclear quantum effects. When tested on models of anharmonic optical and acoustic phonons, we find that classical VDMFT gives good agreement with classical molecular dynamics, including the temperature dependence of phonon frequencies and lifetimes. Using a quantum impurity solver, signatures of nuclear quantum effects are observed at low temperatures.

Introduction. Since the seminal work of the early twentieth century, phonons have been foundational for the description of solids. However, early on it was recognized that anharmonic effects, corresponding to interactions between phonons, were nonnegligible and responsible for a variety of phenomena including thermal expansion, the stability of certain phases, the temperature dependence of phonon frequencies, phonon lifetimes, and thermal conductivity [1–5]. For example, many of the structural and dynamical properties of halide and oxide perovskites have been linked to their soft phonon modes and associated strong anharmonicity [6–11].

Following on the self-consistent phonon theory [2, 12, 13], a number of computational approaches have been developed to simulate the properties of anharmonic solids [14–17], most of which are *static* mean-field theories that seek an optimized harmonic description of anharmonic systems. Therefore, they yield improved thermodynamic properties and shifts in phonon frequencies, but cannot predict phonon lifetimes or non-quasiparticle effects. Such effects can be partially described using perturbation theory [18–23], which fails for strong anharmonicity, or by molecular dynamics [22–26], which is computationally expensive and requires approximate techniques to include nuclear quantum effects [27–30].

Here, we present a vibrational *dynamical* mean-field theory (VDMFT) without the above limitations—it is nonperturbative, exact in the harmonic and molecular limits, systematically improvable through cluster extensions, applicable to problems with or without nuclear quantum effects, and describes phonon spectra. Our VDMFT is completely analogous to conventional DMFT [31–33]: it is a many-body theory of the phonon Green’s function (GF) [34, 35] that maps the dynamics of an anharmonic lattice onto those of a self-consistently defined impurity problem. In this way, VDMFT treats local anharmonicity nonperturbatively. Nonlocal anharmonicity can be included through cluster extensions of DMFT [36, 37] and here we focus on cellular VDMFT.

Theory. Within the Born-Oppenheimer approximation, the vibrational lattice Hamiltonian is

$$H = \sum_{n\alpha} \frac{p_{n\alpha}^2}{2m_\alpha} + \mathcal{V}(\{\mathbf{x}_{n\alpha}\}) \quad (1)$$

where \mathbf{n} are lattice translation vectors and α indexes atoms in the unit cell. Expanding the anharmonic potential energy surface in terms of displacements away from the equilibrium lattice positions, $\mathbf{u}_{n\alpha} = \mathbf{x}_{n\alpha} - \mathbf{x}_{n\alpha}^{(0)}$, naturally leads to an eigenvalue problem for the dynamical matrix

$$[\Omega^2(\mathbf{k})]_{\alpha i, \beta j} = \frac{1}{\sqrt{m_\alpha m_\beta}} \sum_{(\mathbf{m}-\mathbf{n})} e^{i\mathbf{k}\cdot(\mathbf{m}-\mathbf{n})} \Phi_{\mathbf{m}\alpha i, \mathbf{n}\beta j} \quad (2a)$$

$$\Omega^2(\mathbf{k})\mathbf{e}_\lambda(\mathbf{k}) = \Omega_\lambda^2(\mathbf{k})\mathbf{e}_\lambda(\mathbf{k}), \quad (2b)$$

where $\Phi_{\mathbf{m}\alpha i, \mathbf{n}\beta j} = \partial^2 \mathcal{V}(\{\mathbf{x}_{n\alpha}^{(0)}\}) / \partial u_{\mathbf{m}\alpha i} \partial u_{\mathbf{n}\beta j}$ is the force constant matrix, i and j are Cartesian coordinates, and $q_\lambda(\mathbf{k}) = N^{-1/2} \sum_{n\alpha i} \sqrt{m_\alpha} e_{n\alpha i, \lambda}(\mathbf{k}) e^{-i\mathbf{k}\cdot\mathbf{n}} u_{n\alpha i}$ are collective coordinates for phonon branch λ . We note that the dynamical matrix $\Omega^2(\mathbf{k})$ is commonly denoted $\mathbf{D}(\mathbf{k})$ in the literature.

Our object of interest in VDMFT is the finite-temperature phonon GF

$$i\hbar D_{\lambda\lambda'}(\mathbf{k}, t) = \theta(t) \langle [q_\lambda(\mathbf{k}, t), q_{\lambda'}(-\mathbf{k}, 0)] \rangle = 2i\theta(t) C''_{\lambda\lambda'}(\mathbf{k}, t) \quad (3)$$

where $\langle \dots \rangle = \text{Tr}[\dots e^{-H/k_B T}] / Z$ denotes the thermal average, $Z = \text{Tr} e^{-H/k_B T}$ is the canonical partition function, and $C_{\lambda\lambda'}(\mathbf{k}, t) = \langle q_\lambda(\mathbf{k}, t) q_{\lambda'}(-\mathbf{k}, 0) \rangle$ is a one-sided time autocorrelation function. The interacting phonon GF is given by

$$\mathbf{D}(\mathbf{k}, \omega) = \left[(\omega + i\eta)^2 \mathbf{1} - \Omega^2(\mathbf{k}) - 2\Omega(\mathbf{k})\pi(\mathbf{k}, \omega) \right]^{-1}, \quad (4)$$

where $\pi(\mathbf{k}, \omega)$ is the phonon self-energy; henceforth we drop η from our equations.

As usual, in VMDFT we neglect the momentum dependence of the self-energy term $\Omega(\mathbf{k})\pi(\mathbf{k}, \omega) \approx \Omega\pi(\omega)$, which is obtained from a self-consistently defined impurity problem (the impurity frequency matrix Ω will be defined below). The Hamiltonian of the impurity problem is of the Caldeira-Leggett form [38], $H_{\text{imp}} = H_s + H_b + H_{\text{sb}}$ with

$$H_s = \sum_{\alpha} \frac{p_{\alpha}^2}{2m_{\alpha}} + V_{\text{loc}}(\{\mathbf{u}_{\alpha}\}) \quad (5a)$$

$$H_b = \frac{1}{2} \sum_m (p_m^2 + \omega_m^2 q_m^2) \quad (5b)$$

$$H_{\text{sb}} = \sum_{\alpha i m} c_{\alpha i m} u_{\alpha i} q_m, \quad (5c)$$

where (p_m, q_m) are degrees of freedom of a bath of harmonic oscillators and local potential V_{loc} includes anharmonic interactions within the cell. The harmonic bath is completely specified by the hybridization function $\mathbf{\Delta}(\omega)$, which captures the influence of the lattice on the dynamics of the cluster and is defined by

$$2\mathbf{\Omega}\mathbf{\Delta}(\omega) = \omega^2\mathbf{1} - \mathbf{\Omega}^2 - 2\mathbf{\Omega}\mathbf{\pi}(\omega) - \mathbf{D}_C^{-1}(\omega), \quad (6)$$

where $\mathbf{\Omega}^2$ is the impurity dynamical matrix determined by V_{loc} , $\mathbf{D}_C(\omega) = N^{-1} \sum_{\mathbf{k}} \mathbf{D}(\mathbf{k}, \omega)$ is the cellular GF, and N is the number of cells in the Born-von Karman supercell. The impurity Hamiltonian (5) is related to the hybridization by the spectral density $\mathbf{J}(\omega) = -2\mathbf{\Omega}\mathbf{\Delta}''(\omega)$ or

$$J_{\alpha i, \beta j}(\omega) = \frac{\pi}{2} \sum_m \frac{c_{\alpha i, m} c_{\beta j, m}}{\omega_m} [\delta(\omega - \omega_m) - \delta(\omega + \omega_m)]. \quad (7)$$

An accurate treatment of the dynamics of the impurity problem (5) is far more tractable than that of the anharmonic lattice problem. Various impurity solvers, discussed more below, can be used to calculate the anharmonic impurity GF,

$$i\hbar[\mathbf{D}_{\text{imp}}(t)]_{\alpha i, \beta j} = \theta(t)\langle [u_{\alpha i}(t), u_{\beta j}(0)] \rangle, \quad (8)$$

and the harmonic impurity GF $\mathbf{d}_{\text{imp}}(t)$ obtained by neglecting the anharmonicity of the local potential. The phonon self-energy is then

$$2\mathbf{\Omega}\mathbf{\pi}(\omega) = \mathbf{d}_{\text{imp}}^{-1}(\omega) - \mathbf{D}_{\text{imp}}^{-1}(\omega), \quad (9)$$

which defines the lattice GF $\mathbf{D}(\mathbf{k}, \omega)$ within the DMFT approximation. In practice, we make an initial guess of the self-energy and iterate the VDMFT loop until convergence, at which point $\mathbf{D}_C(\omega) = \mathbf{D}_{\text{imp}}(\omega)$. Because cellular DMFT breaks translational symmetry (beyond a single-cell cluster), we periodize the converged self-energy to study lattice quantities [37, 39, 40], as discussed below.

Single-site VDMFT. To illustrate VDMFT, we first consider a one-dimensional chain of oscillators with mass $m = 1$, periodic boundary conditions, and *purely local* quartic anharmonicity,

$$H = \sum_{n=1}^N \left[\frac{p_n^2}{2} + \frac{1}{2} \Omega_0^2 u_n^2 + g u_n^4 \right] + \frac{1}{2} \omega_0^2 \sum_{n=1}^N (u_n - u_{n+1})^2. \quad (10)$$

Physically, this Hamiltonian could model a molecular crystal with anharmonic intramolecular vibrations and harmonic intermolecular vibrations. Here and throughout we assume a fixed lattice constant $a = 1$ and volume Na , such that there is no thermal expansion. We emphasize that, given the exactness of DMFT in infinite dimensions [31, 41], the one-dimensional models studied here provide a challenging test of our VDMFT. The optical phonons of the Hamiltonian (10) are $q_k = N^{-1/2} \sum_n e^{-ikn} u_n$ with dispersion $\omega_k^2 = \Omega_0^2 + 4\omega_0^2 \sin^2(k/2)$. The impurity Hamiltonian has compo-

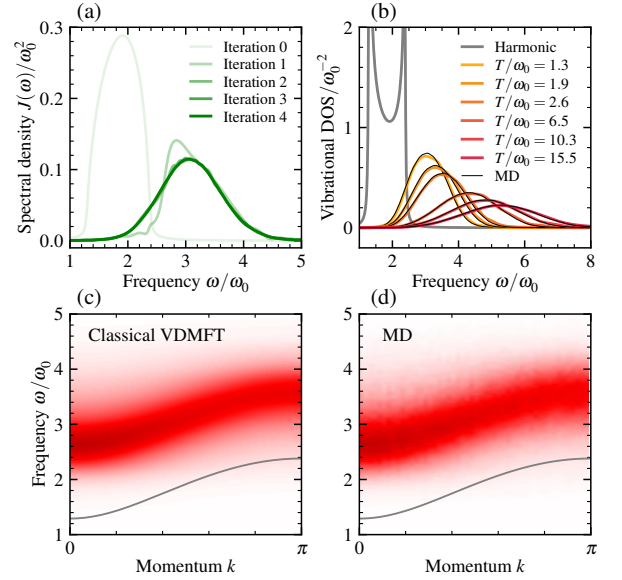


FIG. 1. Single-site VDMFT results for the Hamiltonian (10) with a classical impurity solver. (a) Convergence of the spectral density with DMFT iteration (light to dark). (b) Temperature-dependent density of states (DOS) obtained from harmonic theory (grey), VDMFT (yellow to red), and “exact” molecular dynamics (MD, thin solid black). (c),(d) Spectral functions from VDMFT and MD, respectively, at $T/\omega_0 = 1.3$, compared to the harmonic dispersion (thin grey line). In all results, $\eta/\omega_0 = 0.02$.

nents

$$H_s = \frac{p^2}{2} + \frac{1}{2} \Omega_0^2 u^2 + g u^4 + \omega_0^2 u^2 \equiv \frac{p^2}{2} + V_{\text{loc}}(u) \quad (11a)$$

$$H_b = \frac{1}{2} \sum_m (p_m^2 + \omega_m^2 q_m^2) \quad (11b)$$

$$H_{\text{sb}} = u \sum_m c_m q_m, \quad (11c)$$

where $J(\omega > 0) = (\pi/2) \sum_m c_m^2 / \omega_m \delta(\omega - \omega_m)$. Note that the local potential includes a harmonic term arising from the non-local interaction such that $\Omega = [\Omega_0^2 + 2\omega_0^2]^{1/2}$ is the harmonic impurity frequency.

We first assess the performance of VDMFT with a *classical* impurity solver. In this classical limit, the dynamics of the harmonic bath can be integrated out such that the impurity position satisfies the generalized Langevin equation (GLE),

$$\ddot{u} = -\frac{dV_{\text{eff}}}{du} - \int_0^t ds \gamma(t-s) \dot{u}(s) + \xi(t) \quad (12)$$

where $\gamma(t) = (2/\pi) \int_0^\infty d\omega \cos(\omega t) J(\omega) / \omega$ is a memory kernel, $V_{\text{eff}}(u) = V_{\text{loc}}(u) - \gamma(t=0)u^2/2$ is the local potential with a bath-induced renormalization [42], and $\xi(t)$ is a random force satisfying detailed balance $\langle \xi(t) \xi(s) \rangle = k_B T \gamma(t-s)$. In this formulation, the lattice hybridization can be seen to play the role of a very specific colored-noise thermostat [27, 43]. We solve the GLE numerically [44] to yield an ensemble of trajectories

from which we calculate the classical one-sided impurity autocorrelation function $C_{cl}(t) = \langle u(t)u(0) \rangle$. The impurity GF is then calculated as

$$D_{imp}(t) = -\frac{1}{\hbar\pi}\theta(t)\int_{-\infty}^{\infty}d\omega\sin(\omega t)C_{cl}(\omega)Q(\omega,T) \quad (13)$$

where $Q(\omega,T) = (\hbar\omega/k_B T)(1 - e^{-\hbar\omega/k_B T})^{-1}$ is a temperature-dependent quantum correction factor that makes $D_{imp}(t)$ exact in the harmonic limit [45].

For the Hamiltonian (10), we take the harmonic frequency of the interatomic potential ω_0 as the unit of energy and set $\hbar = k_B = 1$. We use a local harmonic frequency $\Omega_0/\omega_0 = 1.3$ and anharmonicity $g/\omega_0^3 = 4.3$. In Fig. 1(a), we show the spectral density at $T/\omega_0 = 1.3$, which converges after about four iterations to a distribution with a higher average frequency and larger width than the initial noninteracting spectral density. At the same temperature, we show the converged momentum-resolved spectral function $A(k,\omega) = -\pi^{-1}\text{Im}D(k,\omega)$ obtained from VDMFT [Fig. 1(c)] and from exact molecular dynamics (MD) simulations of the full lattice problem [Fig. 1(d)] [46]; the agreement is excellent. As expected, the peaks of the spectral functions are significantly shifted from the harmonic dispersion and are broadened due to phonon lifetime effects. In Fig. 1(b), we show the total vibrational density of states (DOS), $N^{-1}\sum_k A(k,\omega)$, at increasing temperatures ranging from $T/\omega_0 = 1.3$ to $T/\omega_0 = 15.5$. As is well known, the harmonic DOS is independent of temperature. The agreement between VDMFT and MD is seen to be excellent at all temperatures and the DOS shows decreasing lifetimes and phonon hardening with increasing temperature, as expected for a potential with quartic anharmonicity. The remarkable accuracy of single-site VDMFT for this problem can be largely attributed to the purely local form of the anharmonicity.

Next, we consider the possible importance of nuclear quantum effects, which can be straightforwardly included in VDMFT with a *quantum* impurity solver. Here, we use the hierarchical equations of motion [47, 48], which is a numerically exact technique for simulating the dynamics of systems coupled to harmonic baths; technical details are given in the Supplemental Material [49]. In Fig. 2(a), we show the spectral function for the same parameters as in Figs. 1(c),(d); unlike in the classical case, the quantum case is a large many-body problem without a numerically tractable exact solution. We see that the quantum spectral function is narrower and more structured than the classical one, indicating that nuclear quantum effects are indeed important at this temperature.

To understand the origin of the structured spectral features, in Fig. 2, we compare the lattice DOS to the analogous spectrum for a single anharmonic site, i.e., in the atomic or molecular limit. The peaks in the molecular spectrum are due to transitions between adjacent eigenstates of the anharmonic oscillator with intensities depending on their Boltzmann weights and transition matrix elements. These discrete quantum transitions are responsible for the structure seen in the lattice DOS when a quantum impurity solver is used. In Fig. 1(c), we compare the quantum and classical DOS at three temperatures

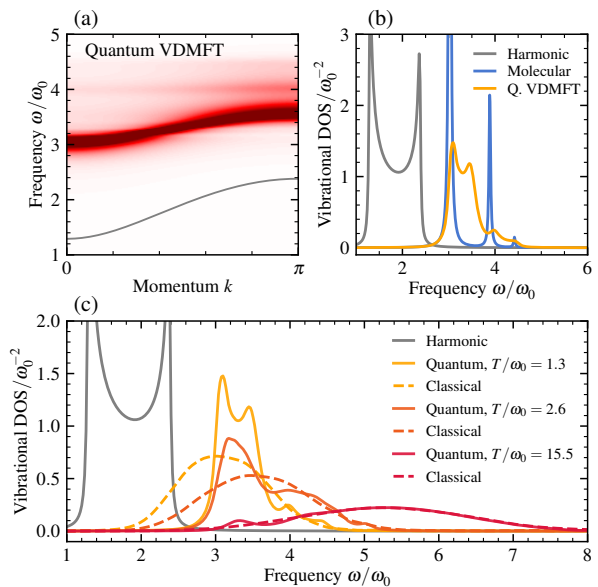


FIG. 2. Single-site VDMFT results for the Hamiltonian (10) with a quantum impurity solver. (a) Quantum spectral function for the same temperature as in Figs. 1(c),(d). (b) At the same temperature, the DOS from harmonic theory (grey), the molecular limit of a single anharmonic oscillator (blue), and quantum VDMFT (yellow). (c) DOS at increasing temperature (yellow to red) obtained by VDMFT with a quantum (solid) and classical (dashed) impurity solver. In all results, $\eta/\omega_0 = 0.02$.

spanning the same range as in Fig. 1(b). At low temperatures, we see the discrepancy due to the importance of nuclear quantum effects. However, at high temperatures, we see that the quantum and classical spectral functions agree due to the diminishing importance of nuclear quantum effects.

Cellular VDMFT. Consider now the vibrational Hamiltonian with *nonlocal* anharmonicity due to a pair potential,

$$H = \sum_{n=1}^N \left[\frac{p_n^2}{2} + V(u_n - u_{n+1}) \right] \quad (14)$$

for which we need the cluster (cellular) extension of VDMFT described above. Due to its invariance to infinitesimal translations, the above Hamiltonian will exhibit a single acoustic phonon branch; the harmonic dispersion is $\omega_k = 2\omega_0 \sin(k/2)$ where ω_0 is the harmonic frequency of the pair potential V .

In two-site cellular VDMFT, we define a symmetry-adapted basis for the cluster impurity problem, $u_{\pm} = (u_1 \pm u_2)/\sqrt{2}$, which diagonalizes the hybridization and decouples the cluster dynamics with impurity Hamiltonian,

$$H_s = \left[\frac{p_{\pm}^2}{2} + \frac{1}{2}\omega_0^2 u_{\pm}^2 \right] + \left[\frac{p_{\mp}^2}{2} + \frac{1}{2}\omega_0^2 u_{\mp}^2 + V(\sqrt{2}u_{-}) \right]. \quad (15)$$

In this impurity Hamiltonian, we have kept only the local, harmonic parts of the nonlocal interactions that cross the boundary of the cluster. In principle, we could also keep local, anharmonic parts of these interactions. However, doing so

breaks the symmetry associated with infinitesimal translations and incorrectly opens a gap at the Γ point (note that periodization only restores *lattice* translational symmetry). Because only the relative coordinate u_- experiences an anharmonic potential, the only nonzero matrix element of the impurity self-energy is $\pi_{--}(\omega)$, which can be obtained numerically using the same classical or quantum impurity solvers described in the previous section. After convergence of the DMFT cycle, we calculate the momentum-resolved spectral function using a periodized self-energy term [37, 39, 40],

$$\Omega(k)\pi(k, \omega) = \frac{1}{2} \sum_{\alpha, \beta=1}^2 [\Omega\pi(\omega)]_{\alpha\beta} e^{ik(\alpha-\beta)}, \quad (16)$$

although other choices are possible [52, 53].

Results of two-site cellular VDMFT are shown in Fig. 3 using a Lennard-Jones pair potential with its minimum at the lattice spacing and its harmonic frequency ω_0 taken as the unit of energy. For simplicity, the potential is truncated to include only cubic and quartic anharmonicity. Results are shown at temperature $T/\omega_0 = 1.2$. In Figs. 3(a)-(c), We compare the momentum-resolved spectral function obtained by cellular VDMFT using a classical impurity solver [Fig. 3(a)], VDMFT using a quantum impurity solver [Fig. 3(b)], and classical lattice MD [Fig. 3(c)]; in Fig. 3(d), we compare the vibrational DOS. Although cellular VDMFT with a classical impurity solver gives a qualitatively correct frequency shift and phonon lifetime, we see that the agreement with lattice MD is not as good as was seen for the previous model of an optical phonon with local anharmonicity. The MD result shows a frequency shift that is about twice as large as that predicted by VDMFT. This can be understood due to the nonlocal anharmonicity in the present model, which requires larger cluster sizes to be quantitatively captured by cellular VDMFT. Although the results are not converged with respect to cluster size, we see a deviation between the quantum and classical VDMFT, indicating that nuclear quantum effects, which are neglected in the MD, are important for these parameters. Like for the model of optical phonons, the features of the quantum spectral function can be traced to the spectral structure of the anharmonic “diatomic molecule” appearing in the two-site impurity problem.

Conclusions and future work. We have introduced vibrational DMFT, including the theory of a cellular extension, and presented numerical tests on one-dimensional chains of anharmonic oscillators, which provide challenging tests for a method whose accuracy improves in higher dimensions. Future work will test alternative impurity solvers, the convergence with respect to cluster size, and the performance in higher dimensions and for other observables such as the free energy [54, 55] and thermal or electronic conductivities [8, 9, 26, 56, 57]. VDMFT can be extended to atomistic materials, either with low-energy Hamiltonians [58, 59] or in a fully ab initio framework. In the latter case, force-fields or electronic structure theory can be used to determine the anharmonic potential energy surface and the anharmonic impurity problem can be solved using thermostatted MD [27, 43] or ef-

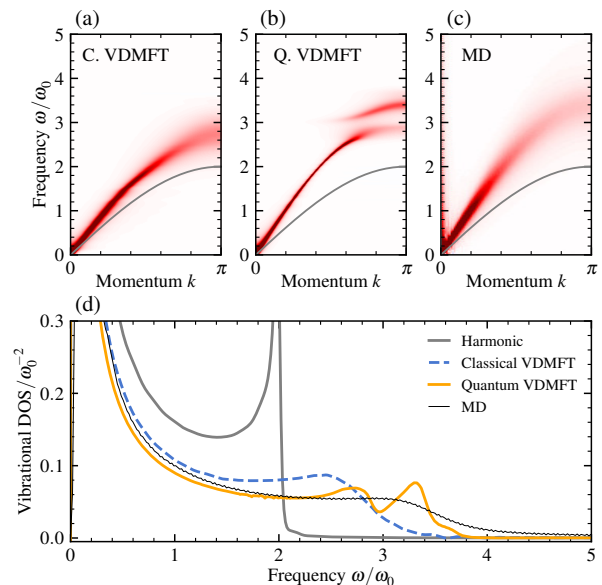


FIG. 3. Two-site cellular VDMFT results for the Hamiltonian (14) with a Lennard-Jones potential truncated at fourth order. (a),(b),(c) Spectral functions from classical VDMFT, quantum VDMFT, and classical MD, respectively, at $T/\omega_0 = 1.2$, compared to the harmonic dispersion (thin grey line). (d) At the same temperature, comparison of the vibrational DOS. In all results, $\eta/\omega_0 = 0.01$.

ficient quantum configuration interaction approaches [60, 61]. Work along all of these lines is currently in progress.

This work was supported in part by the Air Force Office of Scientific Research under AFOSR Award No. FA9550-19-1-0405 and by the National Science Foundation Cyberinfrastructure for Sustained Scientific Innovation program under Award No. OAC-1931321. We acknowledge computing resources from Columbia University’s Shared Research Computing Facility project, which is supported by NIH Research Facility Improvement Grant 1G20RR030893-01, and associated funds from the New York State Empire State Development, Division of Science Technology and Innovation (NYSTAR) Contract C090171, both awarded April 15, 2010. The Flatiron Institute is a division of the Simons Foundation.

* tim.berkelbach@gmail.com

- [1] H. R. Clyde and M. L. Klein, *Crit. Rev. Solid State Mater. Sci.* **2**, 181 (1971).
- [2] M. L. Klein and G. K. Horton, *J. Low Temp. Phys.* **9**, 151 (1972).
- [3] H. J. Maris, *Rev. Mod. Phys.* **49**, 341 (1977).
- [4] B. Fultz, *Prog. Mater. Sci.* **55**, 247 (2010).
- [5] G. Grimvall, B. Magyari-Köpe, V. Ozoliņš, and K. A. Persson, *Rev. Mod. Phys.* **84**, 945 (2012).
- [6] O. Yaffe, Y. Guo, L. Z. Tan, D. A. Egger, T. Hull, C. C. Stoumpos, F. Zheng, T. F. Heinz, L. Kronik, M. G. Kanatzidis, J. S. Owen, A. M. Rappe, M. A. Pimenta, and L. E. Brus, *Phys.*

- Rev. Lett.* **118**, 136001 (2017).
- [7] A. Marronnier, H. Lee, B. Geffroy, J. Even, Y. Bonnassieux, and G. Roma, *J. Phys. Chem. Lett.* **8**, 2659 (2017).
- [8] J.-J. Zhou, O. Hellman, and M. Bernardi, *Phys. Rev. Lett.* **121** (2018), 10.1103/physrevlett.121.226603.
- [9] A. Gold-Parker, P. M. Gehring, J. M. Skelton, I. C. Smith, D. Parshall, J. M. Frost, H. I. Karunadasa, A. Walsh, and M. F. Toney, *Proc. Natl. Acad. Sci.* **115**, 11905 (2018).
- [10] C. Gehrman and D. A. Egger, *Nat. Commun.* **10**, 3141 (2019).
- [11] J. Klarbring, O. Hellman, I. A. Abrikosov, and S. I. Simak, *Phys. Rev. Lett.* **125**, 045701 (2020).
- [12] D. J. Hooton, *Philos. Mag.* **3**, 49 (1958).
- [13] N. R. Werthamer, *Phys. Rev. B* **1**, 572 (1970).
- [14] P. Souvatzis, O. Eriksson, M. I. Katsnelson, and S. P. Rudin, *Phys. Rev. Lett.* **100**, 095901 (2008).
- [15] P. Souvatzis, O. Eriksson, M. Katsnelson, and S. Rudin, *Comput. Mater. Sci.* **44**, 888 (2009).
- [16] O. Hellman, P. Steneteg, I. A. Abrikosov, and S. I. Simak, *Phys. Rev. B* **87**, 104111 (2013).
- [17] I. Errea, M. Calandra, and F. Mauri, *Phys. Rev. B* **89**, 064302 (2014).
- [18] A. A. Maradudin and A. E. Fein, *Phys. Rev.* **128**, 2589 (1962).
- [19] R. Cowley, *J. Phys.* **26**, 659 (1965).
- [20] P. G. Klemens, *Phys. Rev.* **148**, 845 (1966).
- [21] J. Menéndez and M. Cardona, *Phys. Rev. B* **29**, 2051 (1984).
- [22] J. E. Turney, E. S. Landry, A. J. H. McGaughey, and C. H. Amon, *Phys. Rev. B* **79**, 064301 (2009).
- [23] T. Sun, X. Shen, and P. B. Allen, *Phys. Rev. B* **82**, 224304 (2010).
- [24] A. J. C. Ladd, B. Moran, and W. G. Hoover, *Phys. Rev. B* **34**, 5058 (1986).
- [25] K. V. Tretyakov and S. Scandolo, *J. Chem. Phys.* **120**, 3765 (2004).
- [26] N. de Koker, *Phys. Rev. Lett.* **103**, 125902 (2009).
- [27] M. Ceriotti, G. Bussi, and M. Parrinello, *Phys. Rev. Lett.* **103**, 030603 (2009).
- [28] H. Dammak, Y. Chalopin, M. Laroche, M. Hayoun, and J.-J. Greffet, *Phys. Rev. Lett.* **103**, 190601 (2009).
- [29] M. Rossi, P. Gasparotto, and M. Ceriotti, *Phys. Rev. Lett.* **117**, 115702 (2016).
- [30] B. Cheng, A. T. Paxton, and M. Ceriotti, *Phys. Rev. Lett.* **120** (2018), 10.1103/physrevlett.120.225901.
- [31] A. Georges and G. Kotliar, *Phys. Rev. B* **45**, 6479 (1992).
- [32] A. Georges, G. Kotliar, W. Krauth, and M. J. Rozenberg, *Rev. Mod. Phys.* **68**, 13 (1996).
- [33] D. Vollhardt, *Ann. Phys.* **524**, 1 (2011).
- [34] R. Cowley, *Adv. Phys.* **12**, 421 (1963).
- [35] G. D. Mahan, *Many-Particle Physics* (Springer US, 2000).
- [36] M. H. Hettler, M. Mukherjee, M. Jarrell, and H. R. Krishnamurthy, *Phys. Rev. B* **61**, 12739 (2000).
- [37] G. Kotliar, S. Y. Savrasov, G. Pálsson, and G. Biroli, *Phys. Rev. Lett.* **87**, 186401 (2001).
- [38] A. Caldeira and A. Leggett, *Physica A* **121**, 587 (1983).
- [39] O. Parcollet, G. Biroli, and G. Kotliar, *Phys. Rev. Lett.* **92**, 226402 (2004).
- [40] M. Civelli, M. Capone, S. S. Kancharla, O. Parcollet, and G. Kotliar, *Phys. Rev. Lett.* **95**, 106402 (2005).
- [41] W. Metzner and D. Vollhardt, *Phys. Rev. Lett.* **62**, 324 (1989).
- [42] U. Weiss, *Quantum Dissipative Systems* (World Scientific Publishing Company, 2012).
- [43] M. Ceriotti, G. Bussi, and M. Parrinello, *J. Chem. Theory Comput.* **6**, 1170 (2010).
- [44] M. Tuckerman and B. J. Berne, *J. Chem. Phys.* **98**, 7301 (1993).
- [45] J. S. Bader and B. J. Berne, *J. Chem. Phys.* **100**, 8359 (1994).
- [46] MD simulations were performed with periodic lattices of 100-200 sites and time correlation functions were calculated by averaging over an ensemble of up to 60,000 trajectories with initial conditions generated by Metropolis Monte Carlo.
- [47] Y. Tanimura and R. Kubo, *J. Phys. Soc. Jpn.* **58**, 101 (1989).
- [48] A. Ishizaki and Y. Tanimura, *J. Phys. Soc. Jpn.* **74**, 3131 (2005).
- [49] See Supplemental Material at [insert link] for further details of the quantum impurity solver, which includes Refs. [50-51].
- [50] J. C. Light, I. P. Hamilton, and J. V. Lill, *J. Chem. Phys.* **82**, 1400 (1985).
- [51] H. Liu, L. Zhu, S. Bai, and Q. Shi, *J. Chem. Phys.* **140**, 134106 (2014).
- [52] T. D. Stanescu and G. Kotliar, *Phys. Rev. B* **74**, 125110 (2006).
- [53] S. Sakai, G. Sangiovanni, M. Civelli, Y. Motome, K. Held, and M. Imada, *Phys. Rev. B* **85**, 035102 (2012).
- [54] L. J. Sham, *Phys. Rev.* **139**, A1189 (1965).
- [55] N. M. Plakida and T. Siklós, *Acta Phys. Acad. Sci. Hung.* **45**, 37 (1978).
- [56] J. W. L. Pang, W. J. L. Buyers, A. Chernatynskiy, M. D. Lumsden, B. C. Larson, and S. R. Phillpot, *Phys. Rev. Lett.* **110**, 157401 (2013).
- [57] B. Liao, B. Qiu, J. Zhou, S. Huberman, K. Esfarjani, and G. Chen, *Phys. Rev. Lett.* **114**, 115901 (2015).
- [58] X. Ai, Y. Chen, and C. A. Marianetti, *Phys. Rev. B* **90**, 014308 (2014).
- [59] Y. Chen, X. Ai, and C. Marianetti, *Phys. Rev. Lett.* **113**, 105501 (2014).
- [60] M. Neff and G. Rauhut, *J. Chem. Phys.* **131**, 124129 (2009).
- [61] J. H. Fetherolf and T. C. Berkelbach, *J. Chem. Phys.* **154**, 074104 (2021).

Supplemental Material: Anharmonic Lattice Dynamics from Vibrational Dynamical Mean-Field Theory

QUANTUM IMPURITY SOLVER

First, we numerically solve the Schrodinger equation for the anharmonic subsystem and keep the lowest N_s eigenstates $\phi_n(u) = \langle u|n\rangle$, depending on temperature. For the results presented in the manuscript, we kept up to $N_s = 18$ eigenstates. The eigenstates are then transformed to a discrete variable representation [50], $|d\rangle = \sum_n U_{nd}|n\rangle$ that diagonalizes the position operator and thus makes the system-bath Hamiltonian diagonal,

$$H_s = \sum_{dd'} |d\rangle H_{dd'} \langle d'| \quad (\text{S1a})$$

$$H_{\text{sb}} = \sum_d |d\rangle u_d \langle d| \sum_m c_m q_m \quad (\text{S1b})$$

where $u_d = \int du u |\phi_d(u)|^2$. The quantum correlation function is then calculated as $\langle A(t)A(0) \rangle$ where $A = \sum_d |d\rangle u_d \langle d|$.

To simulate the quantum dynamics of a subsystem linearly coupled to a bath of harmonic oscillators, we use the hierarchical equations of motion method [47, 48]. The spectral density of the bath is numerically fit to a sum of (up to) eight Lorentzian modes [51]. To simulate the thermal correlation function, we first propagated the system and auxiliary density matrices starting from a factorized initial condition, until reaching equilibrium; this set of density matrices was then used as the initial condition for the dynamics of the correlation function. All results were found to be converged with the hierarchy truncated at level $L = 4$ and $K = 0$ Matsubara frequencies.